Characterizing the hierarchical structures of bioactive sol −gel silicate glass and hybrid scaffolds for bone regeneration

R. A. Martin, S. Yue, J. V. Hanna, P. D. Lee, R. J. Newport, M. E. Smith and J. R. Jones

References	**This article cites 85 articles, 3 of which can be accessed free** http://rsta.royalsocietypublishing.org/content/370/1963/1422.full.html#ref-list-1 **Article cited in:** http://rsta.royalsocietypublishing.org/content/370/1963/1422.full.html#related-urls

Subject collections	Articles on similar topics can be found in the following collections
	
	   biomedical engineering (122 articles)
	   materials science (95 articles)

Email alerting service	Receive free email alerts when new articles cite this article - sign up in the box at the top right-hand corner of the article or click **here**

To subscribe to *Phil. Trans. R. Soc. A* go to:
http://rsta.royalsocietypublishing.org/subscriptions

REVIEW

Characterizing the hierarchical structures of bioactive sol–gel silicate glass and hybrid scaffolds for bone regeneration

By R. A. Martin[1,*], S. Yue[2], J. V. Hanna[3], P. D. Lee[4], R. J. Newport[5], M. E. Smith[3] and J. R. Jones[2]

[1]*School of Engineering and Applied Science, Aston Research Centre for Healthy Ageing, Aston University, Birmingham B4 7ET, UK*
[2]*Department of Materials, Imperial College London, London SW7 2AZ, UK*
[3]*Department of Physics, University of Warwick, Coventry CV4 7AL, UK*
[4]*School of Materials, University of Manchester, Manchester M1 7HS, UK*
[5]*School of Physical Sciences, University of Kent, Canterbury CT2 7NH, UK*

Bone is the second most widely transplanted tissue after blood. Synthetic alternatives are needed that can reduce the need for transplants and regenerate bone by acting as active temporary templates for bone growth. Bioactive glasses are one of the most promising bone replacement/regeneration materials because they bond to existing bone, are degradable and stimulate new bone growth by the action of their dissolution products on cells. Sol–gel-derived bioactive glasses can be foamed to produce interconnected macropores suitable for tissue ingrowth, particularly cell migration and vascularization and cell penetration. The scaffolds fulfil many of the criteria of an ideal synthetic bone graft, but are not suitable for all bone defect sites because they are brittle. One strategy for improving toughness of the scaffolds without losing their other beneficial properties is to synthesize inorganic/organic hybrids. These hybrids have polymers introduced into the sol–gel process so that the organic and inorganic components interact at the molecular level, providing control over mechanical properties and degradation rates. However, a full understanding of how each feature or property of the glass and hybrid scaffolds affects cellular response is needed to optimize the materials and ensure long-term success and clinical products. This review focuses on the techniques that have been developed for characterizing the hierarchical structures of sol–gel glasses and hybrids, from atomic-scale amorphous networks, through the covalent bonding between components in hybrids and nanoporosity, to quantifying open macroporous networks of the scaffolds. Methods for non-destructive *in situ* monitoring of degradation and bioactivity mechanisms of the materials are also included.

Keywords: bioactive glass; sol–gel; bone regeneration; scaffolds; tissue engineering

*Author for correspondence (r.a.martin@aston.ac.uk).

1. Introduction

Bone is the most widely transplanted material, with the exception of blood [1]. More than 2.2 million bone graft operations are performed annually worldwide in order to repair bone defects in orthopaedics and dentistry [2,3]. Autografts are the preferred choice; being natural tissue, they have the natural structure of bone (although maybe not the same as that required in the bone defect), and contain bone and blood vessel cells as well as progenitor cells plus all the natural growth factors and cells necessary for successful remodelling (regeneration) of the bone [3]. Bone tissue is typically harvested from the iliac crest (upper hip) owing to ease of access. However, autografts require an additional operation to harvest first the healthy bone. Then, the donor site has to be repaired, usually with allograft (treated bone from cadavers) or synthetic bone graft. Furthermore, autograft harvesting is associated with a 20 per cent risk of complication, including infection, nerve damage and chronic pain at the donor site [3–5], which can lead to revision surgery. The limited amount of donor bone available from the patient means that, for large defects, allograft or synthetics are used, with autograft as bone graft extenders. A disadvantage of allograft is its poor mechanical properties [6–8]. Consequently, there is a significant requirement for artificial bone graft materials. Despite there being a large number of synthetic bone grafts available on the market, mostly based on calcium phosphates, synthetic materials are used in only 10 per cent of grafting procedures because they are considered to be inferior to autograft or allograft [2]. Most products are designed to be bioactive such that they stimulate a specific biological response at the material surface, which results in the formation of a bond between the tissues and the material and the formation of new bone. An example is synthetic hydroxyapatite (HA), whose composition is similar to that of bone mineral. Further advances in the material design and understanding of the cell–material interactions are needed. To achieve that, a fuller understanding of the material structure and properties is needed.

Bioactive glasses are one of the most promising synthetic bone replacement materials available because they have the potential to be more bioactive than calcium phosphate-based materials. Bioactive glasses, developed by Hench in 1969 [9,10], bond to bone and stimulate new bone growth even away from the glass–bone interface [11]. A direct comparison with HA *in vivo* has shown that the original melt-derived Bioglass forms a more rapid and stronger bond with bone [12,13]. Bioglass (46.1% SiO_2, 24.4% Na_2O, 26.9% CaO, and 2.6% P_2O_5, in mol%) has been in clinical use since 1985 and has been used in over a million operations as Perioglas (dental) and NovaBone (orthopaedics) particulates (NovaBone LLC, Alachua, FL, USA), but its commercial use has been limited owing to processing limitations. In order to produce a scaffold from glass frit or powder, a sintering process is required, which means the glass must be raised above its glass transition temperature (T_g); however, the 45S5 Bioglass begins to crystallize as soon as its T_g is surpassed, creating a glass–ceramic that can lead to a reduction in bioactivity or unpredictable degradation behaviour [14]. New compositions have been developed to increase the sintering window, but this has so far led to a reduction in bioactivity [15,16].
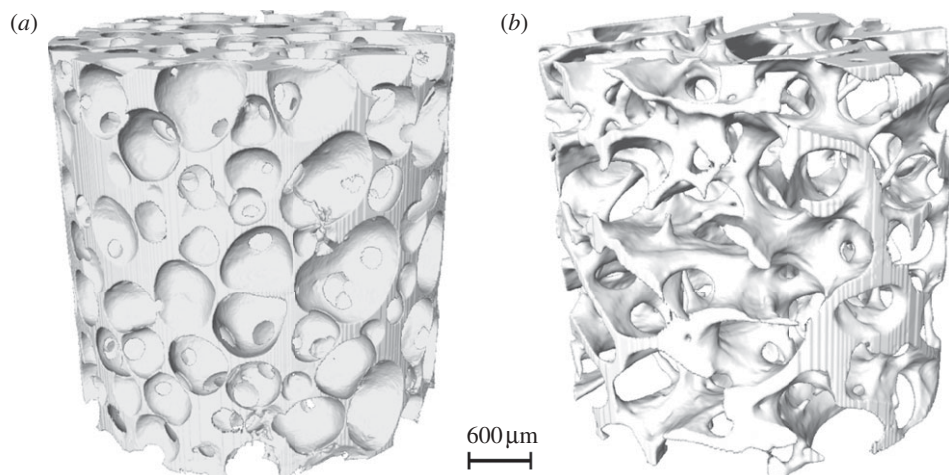
Figure 1. X-ray microtomography images of (*a*) bioactive glass foam scaffold and (*b*) trabecular bone from a human femur proximal to the knee.

Sol–gel-derived glass scaffolds were developed by Li *et al.* [17] with a view to increasing the degradation rate, owing to the high inherent surface area of sol–gel glasses, and allowing glasses to be bioactive with higher silica content (melt-derived glasses are not bioactive above 60 mol% SiO_2) with few compositional components. The enhanced bioactivity of sol–gel glasses over melt–quench glasses of similar composition was originally attributed to the enhanced surface area (two orders of magnitude higher than that of the melt glasses [18]) provided by the nanoporosity that is inherent to the sol–gel process, but later the atomic structure was found to be the real key to this, as described in §3*c*.

Sol–gels can also be processed via a foaming method to produce macroporous networks suitable for tissue scaffolds that mimic the structure of porous bone (figure 1), while maintaining the nanoporosity [19]. The sol–gel glass scaffolds fulfil most of the criteria for a bioactive scaffold, except for one: they are as brittle as the other bioceramic bone graft replacement materials. The sol–gel process also provides a strategy for decreasing the brittleness of the scaffolds. Inorganic/organic hybrids can be synthesized by introducing a polymer into the sol–gel process at an early stage. A hybrid is defined here as the combination of materials, where the organic and inorganic components are not distinguishable above the submicrometre scale [20]. This study reviews sol–gel silicate glass scaffolds and sol–gel hybrids as potential synthetic bone grafts, focusing on the importance of understanding how their hierarchical structure affects their properties and cellular response. The latest developments in characterizing these complex amorphous materials are described. Although the literature is reviewed, generally the recent work of the Imperial–Kent–Warwick collaboration characterizing the structure of these materials is emphasized.

2. An ideal scaffold

The criteria for an ideal scaffold for bone regeneration are that it [8,21,22]:

(i) is biocompatible (not cytotoxic),

(ii) bonds with the existing host bone, creating a stable interface without the formation of fibrous scar tissue,

(iii) acts as a template for three-dimensional bone growth,

(iv) has an interconnected porous network with diameters in excess of $100\,\mu m$ to allow cell penetration and blood vessels to grow in [23],

(v) exhibits mechanical properties such that it can share load with the host bone,

(vi) resorbs at the same rate as that at which the new bone remodels, with dissolution products that are non-toxic and easy to excrete from the body,

(vii) has a surface suitable for osteogenic cell attachment,

(viii) stimulates bone cells and progenitor cells to produce new bone,

(ix) can be shaped prior to implantation to fit the bone defect, and

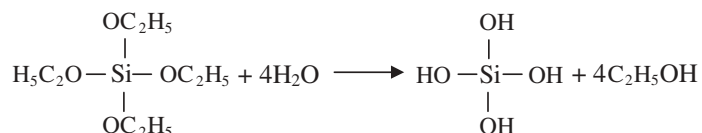(x) can be commercially produced and sterilized for clinical use.

3. Bioactive sol–gels

Sol–gel-derived glasses have many advantages compared with their melt–quench derivatives [24]. Sol–gels are prepared using a low-temperature hydrolysis and condensation process, described in §3*a*. The solution chemistry allows the chemicals to be easily mixed, ensuring good homogenization and uniformity. The lower reaction temperatures can prevent potential crystallization and phase separation, thus allowing glasses to be formed that cannot normally be prepared. The aqueous method results in a large number of residual hydroxyl groups (which aid bioactivity), of which some remain even after the thermal stabilization processing. However, inhomogeneity and phase separation can occur if the conditions are not carefully controlled, but detection of inhomogeneity and phase separation requires advanced atomic characterization techniques in amorphous materials.

(*a*) *Sol–gel preparation*

Sol–gels are prepared using a hydrolysis–condensation reaction, followed by ageing, drying and thermal stabilization processes. Porous scaffolds are produced by agitating the sol with a surfactant, as shown in figure 2 [25,26]. Silicon is typically introduced in the form of tetraethoxysilane (TEOS), $Si(OCH_2CH_3)_4$. The prototypical bioactive sol–gel glasses such as 70S30C (70 mol% SiO_2, 30 mol% CaO) traditionally incorporate calcium in the form of calcium nitrate with a nitric acid catalyst, although more recently alternative precursors have been proposed (§3*c*).

The chemicals are added together and dissolved in a common solvent, usually water, sometimes with some ethanol added. After mixing, a sol is formed, which is a colloidal solution consisting of solid particles suspended in a liquid. During sol formation, the TEOS undergoes a hydrolysis reaction, creating silanol (Si–OH) groups:

$$
\begin{array}{ccc}
OC_2H_5 & & OH \\
| & & | \\
H_5C_2O-Si-OC_2H_5 + 4H_2O \longrightarrow HO-Si-OH + 4C_2H_5OH \\
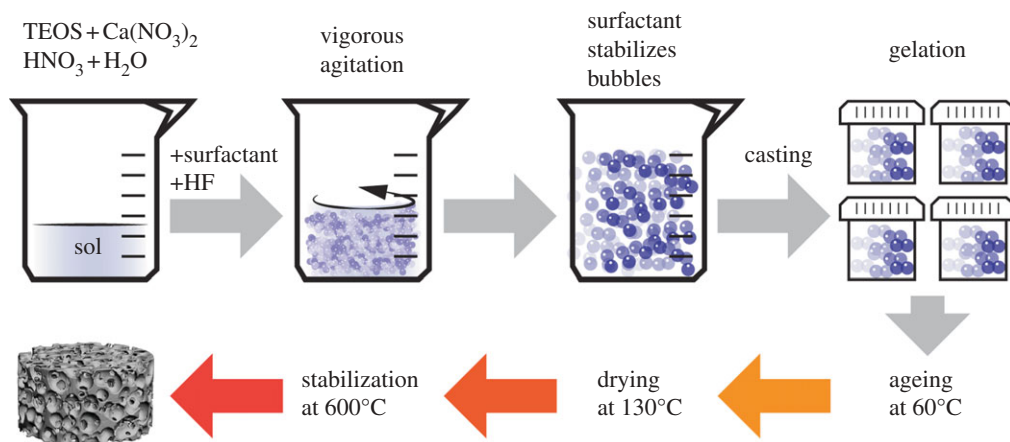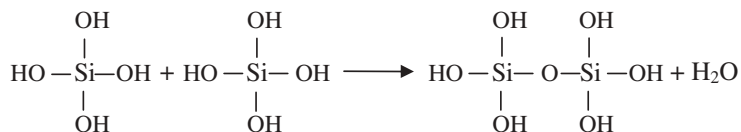| & & | \\
OC_2H_5 & & OH
\end{array}
$$

Figure 2. Schematic of the sol–gel foaming process. (Online version in colour.)

The hydrated silica interacts in a condensation reaction forming Si–O–Si bonds:

If monoliths or foams are being synthesized, acid-catalysed hydrolysis is used. Figure 3 shows an illustration of the formation of a bioactive sol–gel glass. Early in the condensation reactions, silica nanoparticles begin to form. These primary particles then grow and coalesce. As they coalesce, further condensation reactions between surface silanol groups bond the particles together. The viscosity of the sol increases and eventually gelation occurs, with the gel point given by a sharp increase in viscosity. During the ageing process, the aqueous gel continues to cross-link the silicate structure, resulting in the formation of a network glass. After ageing, the gel consists of a three-dimensional network of bonded nanoparticles with the aqueous condensation by-products trapped in the interstitial spaces. The drying stage involves removing the by-products to form a dry monolith. Finally, the monolith is heat-treated or stabilized to strengthen the sol–gel glass through the removal of excess $-OH$ groups and by aiding the incorporation of Ca into the silicate glass network to form a single-phase glass. Figure 3 illustrates that, when calcium is incorporated using calcium nitrate, the calcium is not incorporated until the stabilization process. This has an impact in terms of synthesizing a homogeneous glass, but is even more critical in the low-temperature synthesis of hybrids, in which they are not heated above $60°C$, and will be discussed further in §3f. If nano- or submicrometre particles are required, a basic catalyst is used [28], which terminates the condensation reaction, leaving small spherical particles. Full details on each step of the sol–gel process can be found in Hench & West [29].

   The concentration of $-OH$ groups present in the resulting sol–gel is dependent on the $H_2O/TEOS$ ratio and stabilization temperatures employed. Duran *et al.* [30] reported that a $H_2O/TEOS$ ratio of 1 was insufficient to complete
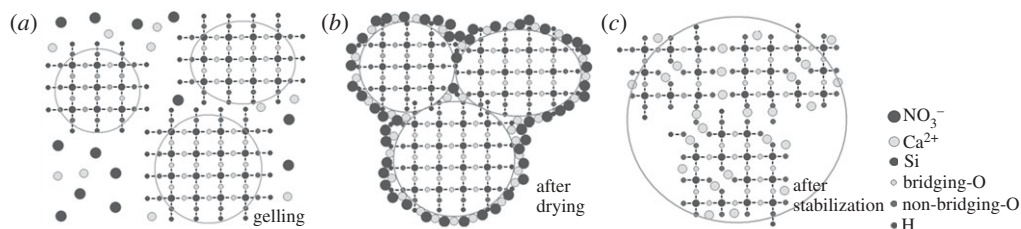
Figure 3. Schematic of the sol–gel process for CaO–SiO$_2$ monoliths, modified from Lin *et al.* [43].

the hydrolysis, ratios of 4 resulted in a complete hydrolysis forming chain-like structures and ratios of 20 resulted in a complete hydrolysis consisting of rings, thus resulting in a three-dimensional network. The rate of gelation is also highly dependent on the temperature and the type of acid catalyst present. Colby *et al.* [31] reported that the rate of gelation increased by a factor of almost 20 when gelling at 70°C compared with 25°C in the TEOS system, while replacing HCl with HF reduced the gelling time from 20 h to half an hour. The role of HF is critical in foam production. Sepulveda *et al.* [32] developed sol–gels with interconnect macropores between 10 and 500 μm by adding a surfactant and vigorously agitating. Foam scaffolds are produced by vigorous agitation of the sol prior to gelation. A surfactant is used to lower the surface tension and stabilize the bubbles. However, permanent stabilization of bubbles is due to the HF. Gelation is needed over a period of a few minutes and is achieved with the addition of HF. The rapid increase in viscosity, combined with the surfactant distribution and concentration, creates homogeneous spherical pores. During gelation, the pores shrink and rupture at the contact points between pores, creating an interconnected structure. Further details concerning the sol–gel process are given in the classic text by Scherer & Brinker [33].

(b) The bioactivity of glasses

The atomic structure determines the dissolution rate of ions, which are released to stimulate the formation of new bones. The atomic structure, therefore, directly affects both the resorption rate (note that the rate of dissolution should closely match the rate of new bone formation and remodelling, as per condition (vi) in §2) and the osteogenic properties, through the selected release of these ions, which are essential for stimulating osteoblast activity. Studies have shown that the selective release of Ca, P and soluble silica can stimulate gene transcription in osteoblasts [34,35].

The mechanism of bone bonding is a complex multi-step process [36–39]. The first five steps suggested by Hench *et al.* are as follows.
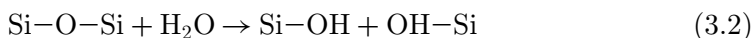
(i) Stage 1

Ion exchange of the cations, Na$^+$ or Ca^{2+}, from the glass with H$^+$ from the surrounding physiological fluid:

$$\mathrm{Si-O-Na + H_2O \rightarrow Si-OH + Na^+_{(aq)} + OH^-} \tag{3.1}$$

(ii) *Stage 2*

The breakage of Si–O–Si bonds is the second step, in which

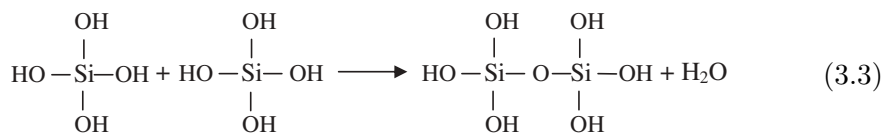$$Si-O-Si + H_2O \rightarrow Si-OH + OH-Si \qquad (3.2)$$

The $Si-O-Si$ are broken to form silanols, releasing soluble $Si(OH)_4$ to the surrounding solution.

The first two stages are highly dependent on the overall composition and type of glass, as discussed below.

(iii) *Stage 3*

Stage 2 results in a high concentration of silanol groups in solution at the glass–solution interface, which can repolymerize to form a silica-rich layer at the glass surface as follows:

$$
\begin{array}{c}
\text{OH} \qquad\qquad \text{OH} \qquad\qquad\qquad \text{OH} \quad\ \text{OH} \\
| \qquad\qquad\ \ | \qquad\qquad\qquad\ \ | \qquad\ \ | \\
\text{HO}-\text{Si}-\text{OH} + \text{HO}-\text{Si}-\text{OH} \longrightarrow \text{HO}-\text{Si}-\text{O}-\text{Si}-\text{OH} + \text{H}_2\text{O} \\
| \qquad\qquad\ \ | \qquad\qquad\qquad\ \ | \qquad\ \ | \\
\text{OH} \qquad\qquad \text{OH} \qquad\qquad\qquad \text{OH} \quad\ \text{OH}
\end{array} \qquad (3.3)
$$

(iv) *Stage 4*

If they are present in the glass composition, Ca^{2+} and PO_4^{3-} groups migrate to the surface, through the silica-rich layer, and precipitate from the solution (or body fluid) to form a $Ca–P_2O_5$-rich film on top of the silica layer. This results in the growth of an amorphous calcium phosphate layer.

(v) *Stage 5*

The amorphous calcium phosphate layer begins to incorporate OH^- and/or CO_3^{2-} anions from the surrounding solutions and crystallizes to form a mixed hydroxycarbonate apatite (HCA) layer. The formation of this biologically active HCA layer is believed to be a prerequisite for glasses and glass ceramics to bond to host tissue.

These five stages have been understood by studying the materials science of bioactive glasses. The stages occur relatively quickly, taking a few hours to a few days, depending on the initial starting composition and the number of $Si-O-Si$ bonds for each Si atom. The reaction has only recently been confirmed, using diffraction studies, which will be discussed in §3c.

The biological interactions at the HCA–tissue interface are less well understood, but are thought to involve protein adsorption; the incorporation of collagen fibrils from the host bone; the attachment of bone progenitor cells; cell differentiation; and the excretion of bone extracellular matrix, followed by its mineralization.

(c) Atomic structure of sol–gel-derived bioactive glass

Calcium is an important component in bioactive glass because it is instrumental in bone bonding, and dissolved calcium is needed to stimulate the cells to produce bone. The role of calcium in the glass network is that of a network modifier.
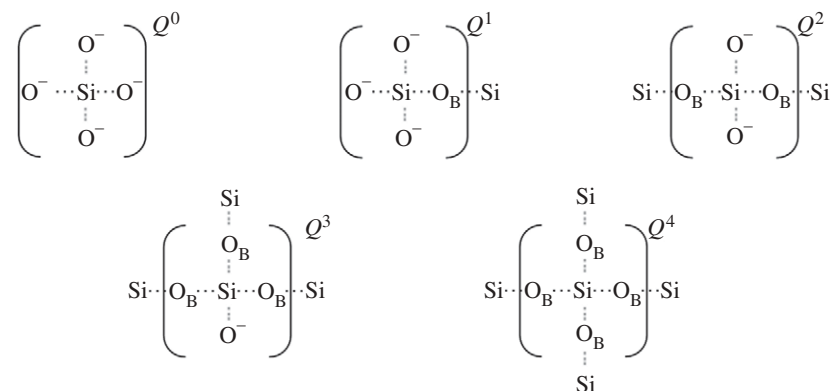
Figure 4. Schematic of the different Q structures that can describe Si network connectivity in glasses. O_B represents a network-forming bridging oxygen bond (Si–O–Si).

Silicon is the network former, and the silica network of bridging oxygen (Si–O–Si) bonds is disrupted by ionic calcium, forming non-bridging oxygen (O_{NB}) bonds (Si–O–Ca). This disruption is necessary for a glass to degrade and be bioactive. As the calcium has a 2^+ charge, it must link to another O_{NB} bond.

Until the late 1980s, the majority of bioactive glasses were melt-derived. The bioactivity of the glasses is known to be dependent on composition, with glasses not being bioactive at silica contents above 60 mol%. This is because changing the composition changes the atomic structure of the glass. Hill [40] proposed that the bioactivity of these glasses could be predicted using a network connectivity (N_c) model. The N_c describes the average number of bridging oxygen atoms per silicon and can range between 0 and 4, as shown in figure 4.

The N_c is typically described as Q^n, where n is the number of bridging oxygen atoms per Si atom. Hill [40] noted that the optimal N_c for melt–quench bioactive glasses is approximately 2 (Bioglass has an N_c of 1.9), with bioactivity being lost above an average N_c of 2.4. However, if the N_c is too low, then the rate of dissolution is too great and the glass dissolves far too rapidly (violating condition (vi) in §2). Thus, the material simply dissolves away and does not provide mechanical support or release the required cations over an intermediate time frame. If N_c is very low, then a glass network will not form during synthesis. In contrast, glasses containing few cations have a high N_c, which inhibits the ion exchange described in stage 1 and the breaking of Si−O−Si bonds described in stage 2, rendering the material bioinert.

Sol–gel-derived glasses can, however, be bioactive with up to 90 mol% SiO_2 [17,41]. This was originally attributed to the high specific surface area and nanoporosity of the sol–gel glasses but, actually, the nature of the atomic structure of sol–gel glasses makes it more complicated. In sol–gel glasses, the N_c is lower than expected from the nominal composition. In fact, H^+ can be considered a network modifier in sol–gel glasses, such that 70S30C is more accurately described as mol% $(SiO_2)_{70}(CaO)_{30}(H_2O)_x$ and it is this high OH content that enables the glass to remain bioactive [27]. The OH arises owing to the silica network forming in an aqueous environment.

The key technique for determining the atomic structure of glass is magic angle spinning solid-state nuclear magnetic resonance (NMR). For example, peak fitting of ^{29}Si NMR spectra can determine the relative percentage of Q structures in a glass. Melt-derived glasses tend to display a single Q structure, e.g. Q^2 for Bioglass [42]; however, sol–gel glasses have a range of Q structures [43]. ^{1}H NMR has enabled the hydrogen content of 70S30C to be determined. Results show that for stabilized 70S30C (after heat-treating to 600°C) the hydrogen content was $6 \times 10^{-3}\,\mathrm{mol\,g^{-1}}$, which equated to an additional 0.38 −OH per silicon atom or silica tetrahedron [43]. This reduces the N_c accordingly. ^{29}Si NMR has determined that foams stabilized at 600°C contain a mixture of Q^4 (48%), Q^3 (24%) and Q^2 (28%), while a HCA layer forms within 8 h. After heat-treating to 800°C in a highly connected network, ^{1}H NMR still reveals a reduced, but significant, OH content [27]. However, despite the high N_c, an HCA layer still forms in simulated body fluid (SBF) within 3 days on the sintered sol–gel-derived glasses. Therefore, it is concluded that in addition to providing additional oxygen atoms, which reduce the N_c, the −OH groups play a far more significant role in terms of the bioactivity even at relatively low concentrations. This is in agreement with studies of apatite deposition on titanium that has been modified to have high concentrations of Ti–OH [44] at the surface and polymers with high concentrations of surface −COOH groups [45].

The majority of 70S30C sol–gels reported in the literature have followed the original method of incorporating calcium into the gel, using a calcium nitrate precursor. Results have shown that calcium is not incorporated into the silicate network until heat-treating beyond 350°C (figure 3). Raman spectra of 70S30C gels contain a peak at $1052\,\mathrm{cm^{-1}}$, which is attributed to nitrate being present. Spectra were collected at different stages of the process. The nitrate peak reduced with temperature until 350°C, when the peak completely disappeared; this is attributed to calcium becoming fully incorporated into the silicate network [46,47]. This result was confirmed by X-ray diffraction (XRD) spectra collected as a function of processing temperature and complementary ^{29}Si NMR studies [43]. The NMR data showed that the N_c of the dried gel was higher (high Q^4 content) for temperatures below 400°C than it was above 400°C when the calcium was incorporated, increasing the Q^3 and Q^2 content. During the mixing stage, the calcium nitrate is soluble in the sol and, during condensation, it remains in solution as the silica nanoparticles form and coalesce (figure 3). During drying, the condensation by-products are driven off, and the calcium nitrate coats the silica nanoparticles. As the temperature increases above 400°C, the calcium enters the network by diffusion, and the nitrate by-products are driven off above 550°C. If large (greater than approx. 1 cm) monoliths are made, this can cause inhomogeneity of the calcium distribution owing to large diffusion distances [48]. This is less prominent in foams as the struts are relatively thin [49]. Note that, even after heat-treating the sol–gel to incorporate the calcium, the processing temperature is still much lower than the processing temperature of melt–quench-derived bioactive glass, which is in the range of 1350–1400°C [50,51].

Computational modelling was also used to examine the effect on 70S30C of increasing amounts of OH present. It was found that increasing the OH content further reduced the silica N_c, as would be anticipated, and that the increase in the number of Ca−OH bonds is approximately balanced by the reduction in the

number of Ca−O$_B$ bonds. These results suggest that calcium distribution becomes more homogeneous with increasing OH content. The simulations were also used to investigate the effects of reducing the density of 70S30C systems, concluding that there is no change in the number of oxygen atoms surrounding Si or the number of O$_{NB}$ atoms surrounding Ca. However, the number of bridging oxygen atoms and hydroxyl groups surrounding Ca decreases [52].

Synchrotron-based XRD and neutron diffraction (ND) are also powerful techniques that can be used to study the structure of amorphous materials. These techniques require major national/international facilities but can provide detailed information on glass structure. Conventional XRD, high-energy X-ray diffraction [53] and ND [54,55] measure the total diffraction pattern. It can sometimes be difficult to determine individual correlations from a single diffraction pattern owing to the overlapping correlation functions. For example, when undertaking diffraction, the Ca–O correlation overlaps with the O−Si−O correlation. However, combining diffraction data with complementary element-specific techniques such as extended X-ray absorption fine structure [56], X-ray absorption near-edge structure [57] or isotopic substitution ND can significantly aid data interpretation. These techniques can be further complemented by solid-state NMR [43,47], Raman and Fourier transform infrared (FTIR) spectroscopy and computational modelling [52,58].

The local calcium environment in crystalline calcium silicates and apatites is particularly diverse. This implies the presence of a range of possible Ca−O correlations, with associated variation in coordination numbers and average separation distance. For example, β-wollastonite (CaSiO$_3$) has three distinct Ca sites with coordination numbers of 6, 6 and 7, respectively [59], whereas calcium nitrate (Ca(NO$_3$)$_2$·H$_2$O) has nine oxygen atoms surrounding a given calcium ion. This makes it particularly challenging when trying to understand the atomic-scale structure in amorphous sol–gel glasses.

To probe the Ca–O environment in 70S30C glass, the method of isotopic substitution applied to ND was employed [54,55]. Two 70S30C samples were prepared, both deuterated to avoid inelastic scattering from hydrogen: one sample contained naturally abundant calcium, whereas the second sample contained enriched [44]Ca. Apart from the isotopic enrichment, both samples were prepared and treated identically, and XRD confirmed that the samples were structurally identical. The isotopic substitution difference method enabled the calcium correlations to be isolated from the more complex total structure. [nat]Ca and [44]Ca have coherent neutron scattering lengths of 4.70 and 1.42 fm, respectively [60]. The total pair correlation function for 70S30C is given in figure 5a, together with markers indicating when the individual overlapping correlations occur. Subtracting the diffraction pattern of the [44]Ca-enriched sample from the natural abundance sample eliminates correlations not containing calcium, thus removing the overlapping O−Si−O correlations as well as the Si−O and O−D correlations, as shown in figure 5b. Results suggest that calcium is in a complex local environment surrounded by a broad distribution of oxygen atoms, which is best modelled using three distinct but partially overlapping correlations centred at 2.3, 2.5 and 2.75 Å. These enriched samples were then exposed to SBF for 30 min before being rerun to enable the calcium environment to be studied during the initial calcium loss (stage 1 of the bioactivity mechanism). The time period of 30 min was selected because this was the point at which
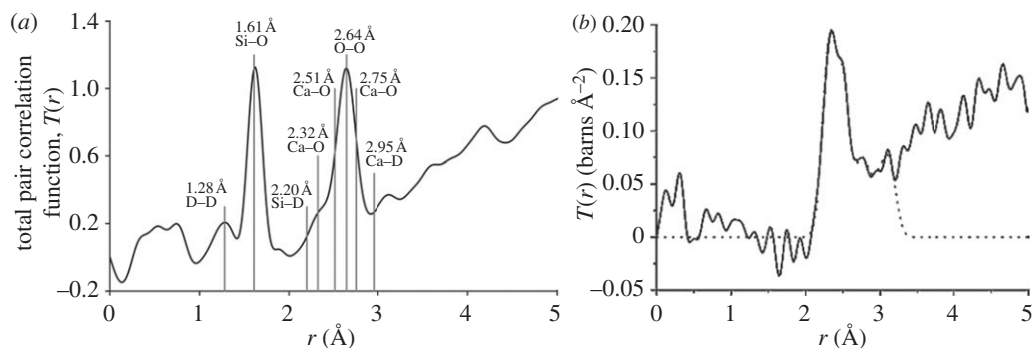
Figure 5. (*a*) Total pair correlation function, $T(r)$, for $(CaO)_{0.3}(SiO_2)_{0.7}$ with the individual pair correlations highlighted and (*b*) difference correlation function with non-Ca terms eliminated [54].

the total calcium content in the gel is at its lowest, i.e. the point at which the maximum Ca content has leached from the glass (stage 1) prior to the Ca re-depositing in the form of an amorphous calcium phosphate (stage 4). The data showed that selective Ca−O correlations are leached from the sol–gel into the surrounding medium, with the shortest correlation at 2.3 Å decreasing in intensity by a factor of 7–8 within 30 min of exposure to SBF. The three Ca−O peaks at 2.3, 2.5 and 2.75 Å were assigned to $Ca−O_{NB}$, Ca−OH and $Ca−O_B$, respectively. Thus, it was concluded that calcium ions associated with O_{NB} atoms are the first to dissociate and enter the surrounding physiological medium. Conversely, the Ca−OH remain almost constant during this period and the number of Ca associated with bridging oxygen atoms increases [55]. Computational molecular dynamics modelling supports the presence of the three distinct Ca−O sites and the presence of hydroxyl groups bonded to silica [52]. These results also show that a significant number of hydroxyl groups are bonded directly to calcium; this is expected to enhance the solubility of Ca and further increase the bioactivity.

In addition to studying the structure and corresponding early stages of dissolution (stages 1 and 2), complementary diffraction studies have been conducted characterizing the formation of the silica-rich layer followed by amorphous calcium phosphate and HCA (stages 3–5) [54,61]. FitzGerald *et al.* [53] designed a sample cell that enables XRD patterns to be continually collected from a 70S30C foam reacting in SBF on a synchrotron beam-line. Key to this was developing a sample holder that could clasp a foam scaffold and allow SBF to circulate while simultaneously collecting X-ray data. Kapton windows were used to produce X-ray transparent windows to the chamber. XRD revealed that, after only 30 min of exposure to SBF, 75 per cent of the calcium content was lost from the bulk of the foam. Fluctuation of calcium content in the material and in the SBF was observed, showing the calcium ions continually being released from the glass and redeposited. After 1 h, growth of calcium octacalcium phosphate crystallites was observed, but, by 10 h, the crystallites were replaced by a disordered phase, which continued to grow. After 25 h, poorly crystalline HA overlaid a (Ca-depleted) silicate glass.

This work was continued by the study of the formation of HCA Bragg peaks using XRD while simultaneously using small-angle X-ray diffraction to monitor the decrease in nanopore diameter as ACP/HCA deposits in these pores [61]. Results have shown that the HCA formation mechanisms proposed for melt–quench glasses by Hench *et al.* are still valid for sol–gel-derived glasses. Using polished flat plate surfaces on melt–quench glasses has enabled the rate of formation of ACP/HCA to be determined. Surface-sensitive shallow angle X-ray diffraction has been employed to study the formation of ACP followed by HA on Bioglass [51]. ACP was detected within 4 h of exposure to SBF and crystalline apatite was detected within 3 days. The ACP was estimated to form a layer approximately 2 μm thick after only 4 h, which increased to a depth of 4 μm after 8 h exposure to SBF. This confirms stages 4 and 5 of the suggested bioactivity mechanism, even if the actual reaction is more complex than first thought. ^{17}O NMR found rapid loss of O_{NB}, as calcium is leached from the glass, which supports the theory of repolymerization of Si–OH groups (stage 3) [54]. The importance of these advanced characterization techniques is illustrated by the conventional XRD and FTIR studies simply observing an apatite layer forming at 8 h of exposure to SBF [19,62]. Scanning electron microscopy (SEM) has been used, in conjunction with XRD and FTIR, to monitor the formation of apatite layers on sol–gel glasses [62–65]. Microfocus techniques have also been employed to map detailed (micrometre resolution) elemental distributions within these glasses and at the glass–biological fluid interface. For example, Lao *et al.* [66–69] used particle-induced X-ray emission associated to Rutherford backscattering spectroscopy to map elements at the glass–biological fluid interface. Using a proton scanning microbeam allowed simultaneous mapping of P, Si, Ca and Mg, and their results revealed the formation of a Ca–P–Mg layer, confirming the bone-bonding ability of their materials. X-ray microfluorescence techniques can also be used to determine and quantify elemental distributions of both major and trace elements [70].

(*d*) *Characterization of macroporous networks*

A scaffold for bone regeneration should act as a three-dimensional template and must contain interconnected pores suitable for vascularization as noted in §2*d*. The size of the interconnects is the critical parameter of the pore network, rather than pore size and percentage porosity. SEM images are often used for this, but they are two-dimensional images of a fracture surface, which means that it is not possible to visualize the maximum pore diameter of each pore, as it is likely to be out of the plane of the image. The field of view is also small. Three-dimensional images of an entire scaffold can be obtained from X-ray microtomography (μCT), which gives qualitative information on pore shape and heterogeneity. Figure 1 shows that the sol–gel glass foam scaffolds have a similar pore size and structure to porous human bone. The user can view through the three-dimensional images and manually measure pores and interconnects using image analysis software. However, image analysis methods are needed that can be applied to an entire scaffold to obtain pore size distributions.

The traditional method for obtaining pore size distributions has been mercury intrusion porosimetry (MIP). The pore diameter obtained is the equivalent diameter of constrictions to the flow of mercury as a function of pressure applied.
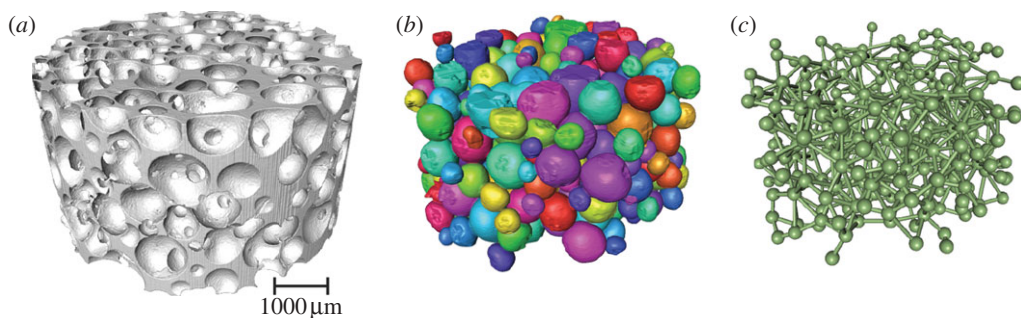
Figure 6. (*a*) X-ray microtomography image of a bioactive glass foam scaffold, (*b*) pores within the scaffold in (*a*) identified by image analysis algorithms and (*c*) a ball and stick representation of the location of macropores (balls) and the paths of connectivity between the pores (sticks). (Online version in colour.)

The technique is destructive, and it is not possible to determine pore shape or what pore size the technique is measuring.

μCT is non-destructive as long as the material is not susceptible to X-rays. However, complex operations are required to obtain pore size distributions from three-dimensional images. An analysis method that combines a series of algorithms has been developed. The algorithms are applied in series to the images in three dimensions to identify the pores and the interconnects, and then obtain the pore and interconnect size distributions [22,49,71,72]. Initially, the macropores are identified (figure 6). This is simple for closed pores, but, for this open pore structure, a new dilation algorithm had to be developed [71]. A dilation algorithm is used to take steps of known size from the pore walls to the centre of the pores. The number of steps are recorded. When the dilation is carried out across the entire sample in three dimensions, a distance map is created. A three-dimensional watershed algorithm is applied to the distance map to identify individual pores (figure 6*b*). A third algorithm groups voxels with neighbours in the same two adjoining pores and they are defined as interconnects. Recently, Yue *et al.* [49] added the step of using principal component analysis to improve the accuracy of interconnect size. This enabled the quantification of the change in interconnect size of a bioactive glass foam scaffold as a function of time of the scaffolds being exposed to SBF while they were subjected to fluid flow [73]. This could be achieved using a flow chamber system because the tomography technique is non-destructive.

The ball and stick image in figure 6*c* illustrates the positions of the centres of the macropores (balls) in figure 6*b* and the sticks show the connectivity of macropores. Together with the size of each pore and interconnect, the connectivity model can be used as an input for pore network analysis for computational fluid simulations [74]. Figure 7 compares interconnect size distributions of a 70S30C bioactive glass scaffold obtained by MIP and μCT image analysis. The distributions show that the image analysis of the μCT determines a higher interconnect size than that measured by mercury porosimetry. This could be due to resolution limitations of the μCT (5 μm in this case), but also due to the mercury porosimetry model applied not accurately measuring actual interconnect diameters.
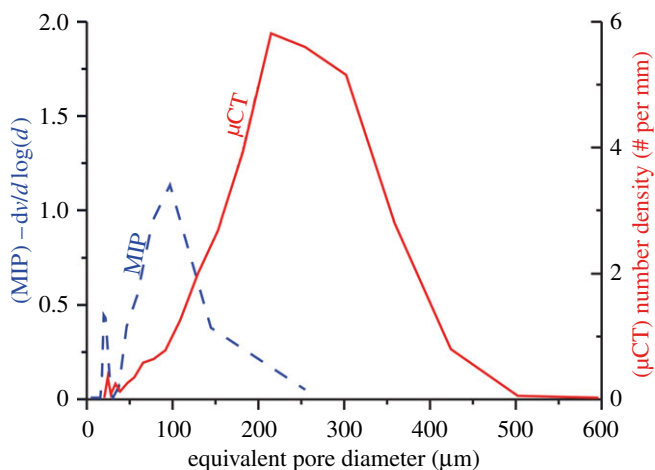
Figure 7. Interconnect pore size distributions of sol–gel foam scaffolds obtained using mercury intrusion porosimetry (MIP) and image analysis of X-ray microtomography images by image analysis algorithms (# refers to number of interconnects). Modified from Jones *et al.* [8]. (Online version in colour.)

(*e*) *Recent advances in sol–gel glass foams*

Following the success of the original sol–gels developed by Li *et al.* [17] and the archetypal 70S30C sol–gel scaffolds, there has been considerable research effort devoted to further improving the system by adding functionality such as incorporating proteins [75] or antibacterial ions, optimizing precursors and developing functional hybrids. By optimizing the sintering process, foam scaffolds were produced with compressive strengths of 2.4 MPa, while maintaining the interconnected pore structure and HCA formation at 3 days in SBF. The original stabilization temperature was 600°C. Sintering above the T_g (approx. 740°C) increased the compressive strength of the sol–gel and reduced the nanoporosity owing to viscous flow and a densification of the silica network [19]. This reduced bioactivity as the dissolution rate decreased.

Surgical site infections can occur during implantation of medical devices. Despite implants being sterilized prior to surgery, microbes are ever present on the patient's skin and can be transferred during surgery. Bioglass has no antibacterial attributes [76]. Consequently, Bellantone *et al.* [77] developed antibacterial Ag-doped sol–gels, containing 2 per cent Ag_2O by weight. The Ag-doped sol inhibited the growth of *Escherichia coli*, *Pseudomonas aeruginosa* and *Staphylococcus aureus* micro-organisms *in vitro* without being toxic to human bone cells. The antibacterial action was attributed solely to the leaching of Ag^+ ions from the glass matrix. Foam scaffolds were then developed of this composition and showed controlled release of Ag without changing the bioactivity of the scaffolds [78].

Lenza *et al.* [79] developed three-dimensional bioactive scaffolds that incorporated proteins on the glass surface, by first functionalizing the glass with aminosilanes. The proteins were released in a controlled manner over a 30 day time period when placed under physiologically representative conditions. The proteins were found to be released at a rate similar to that of the glass dissolution. Coating sol–gel glasses with a layer of protein did not adversely affect bioactivity,

and HCA formation was detected within 5 h of immersion in SBF. Furthermore, the proteins were not denatured during incorporation into the sol–gel and thus offer the potential to release proteins to stimulate the formation and regeneration of bone.

Karakoti *et al.* [80] have developed novel 70S30C sol–gel composites containing nanoparticles of cerium oxide which have been shown to enhance the production of collagen by adult bone marrow-derived human mesenchymal stem cells (HMSCs). After 10 days of culture, the nanoceria composites showed enhanced osteoblast differentiation of HMSCs and collagen production compared with ceria-free scaffolds. It is believed that ceria acts as an oxygen buffer to regulate the differentiation of HMSCs.

(f) Inorganic/organic hybrid foam scaffolds

Although 70S30C sol–gel foams have excellent bioactivity properties and good compressive strengths, they are brittle. Producing a composite of bioactive glass in a degradable polymer matrix is the obvious way to induce toughness in a glass. A problem for conventional composites is that the inactive phase would mask the bioactive phase, so that only those parts protruding from the surface would be in contact with the host bone and provide islands of attachment sites for progenitor cells. Another area of concern is the likelihood of differing degradation rates of the two phases in a conventional composite. Ideally, the two phases should degrade congruently and at a rate that can be controlled depending on the application. However, in conventional composites where microparticles or fibres are dispersed in a polymer matrix, the two phases degrade at different rates. Thus, particles become loose and might cause an immune response. One reason for this is that it is difficult to match the degradation rate of a polymer to a ceramic or glass particle that is encased in the polymer. An alternative strategy is the synthesis of hybrids where the degradable polymer is introduced into the sol stage of the sol–gel foaming process, so that the polymer chains interlock between the nanoparticles of silica while they coalesce. Importantly, the silica network is still continuous in three dimensions [81].

The hypothesis is that the fine-scale interactions between the organic and inorganic chains result in the material behaving as a single phase, leading to controlled congruent degradation and tailored mechanical properties. Interactions at the molecular level mean that when cells approach the surface of the hybrid they will contact the inorganic and organic components simultaneously and the hybrid will retain the biological properties of bioactive glass. Critical for success is obtaining controllable covalent bonding (coupling) between the organic and inorganic components. Without that, the hybrid will dissociate rapidly on contact with water. Advanced probe techniques are again needed to understand the nanostructure of the hybrids.

Mahony *et al.* [82] developed silica–gelatin hybrids with tailorable degradation and mechanical properties. The key to achieving control is obtaining covalent coupling between the gelatin and the silica. Coupling is achieved by functionalizing the gelatin before incorporation into the sol. One reason for choosing gelatin was that it is hydrolysed collagen, which is a component of natural tissue. However, an important advantage of gelatin is that it contains −COOH and −NH groups, which allows it to be functionalized with
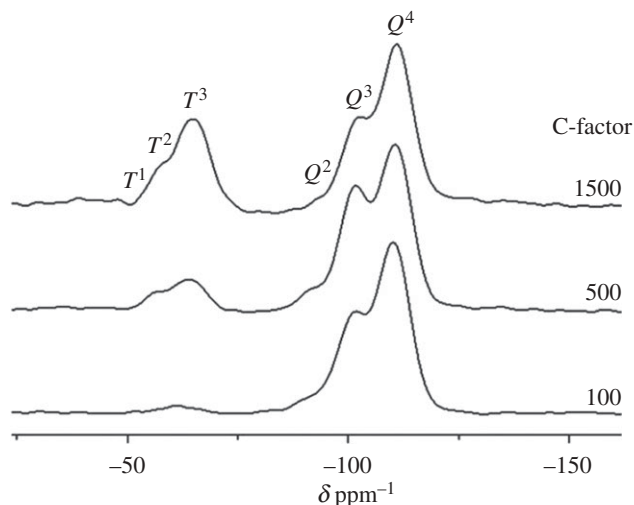
Figure 8. ^{29}Si magic angle spinning NMR for silica–gelatin hybrids (30 wt% gelatin) with a C-factor (molar ratio of coupling agent: gelatin) of 100, 500 and 1500. Spectra indicate T and Q species [82].

glycidoxypropyltrimethoxysilane (GPTMS). The hypothesis was that the epoxy ring on one end of the GPTMS molecule would react with the −COOH group to form covalent bonds. Scaffolds are produced in a method similar to that shown in figure 2, except that there is no thermal stabilization. Scaffolds are gelled and aged at 40°C and freeze-dried. The macropores can be quantified using the three-dimensional image analysis algorithms performed on µCT images.

Degradation studies in SBF showed that, as the amount of coupling between the organic–inorganic phases increases, the amount of gelatin released from the hybrids decreases. This is unsurprising, but the interesting result was that the amount of soluble silica released also decreased, following a trend similar to that of the rate of gelatin release. Both could be controlled between instant dissolution to negligible release depending on the amount of coupling used. This indicates that the covalent coupling between the inorganic and organic phases was successful. This was proved with NMR. ^{29}Si NMR was undertaken to characterize the degree of bonding between the gelatin and silica gel phases. Figure 8 shows some typical ^{29}Si NMR spectra from such hybrids. The Q^n species represent the average number of Si−O−Si bonds per silicon as described in §3c, whereas the T species represent the number of Si−O−Si bonds per silicon for a silicon atom that is bonded to a carbon atom. The C-factor represents the molar ratio of GPTMS: gelatin used during the synthesis. Increasing the covalent coupling increased the relative number of T species at the expense of Q species, indicating strong covalent links between the inorganic and the organic phases. The most common and straightforward NMR methods for characterizing such silicate and hybrid networks are one-dimensional high-resolution experiments. However, NMR approaches are becoming more sophisticated at picking out specific interactions; further details of NMR techniques suitable for studying organic–inorganic interfaces in silica hybrids are given by Babonneau *et al.* [83] and the use of two-dimensional proton-based sequences by Alonso *et al.* [84]. Another aspect

of the advance of NMR methods is the combination of experimental NMR data and first principles calculations to provide additional structural insight, which has been applied to a conventionally formed 45S5 glass by Pedone *et al.* [85].

As discussed earlier, heat-treating to 350°C is required to incorporate calcium fully into the sol–gel when using calcium nitrate precursors. The development of hybrids, many of which contain polymers that would degrade at these high temperatures, has resulted in the need to introduce calcium into the sol–gel using alternative methods. Poologasundarampillai *et al.* [81] attempted to introduce calcium into sol–gel hybrids using calcium chloride. Yu *et al.* [86] undertook a detailed comparison of 70S30C formed using calcium methoxyethoxide, calcium chloride and calcium nitrate precursors, investigating the incorporation of calcium into the network as a function of temperature. XRD and NMR data showed that calcium introduced using calcium methoxyethoxide entered into the silica network at room temperature, whereas the calcium remained as a calcium salt with the other precursors until high temperatures were reached.

4. Summary

Sol–gel bioactive glasses that have enhanced bioactivity and degradation rates compared with melt-derived bioactive glasses and scaffolds with hierarchical pore structures suitable for bone in-growth can be produced by a foaming process. The foams fulfil many of the criteria as ideal scaffolds for bone regeneration; however, in order to characterize their hierarchy, a combination of advanced techniques is needed. In fact, the need to quantify the pore network and understand the atomic structure of these complex amorphous materials and their interactions with body fluid has pushed the boundaries of techniques such as X-ray μCT, X-ray and ND, and solid-state NMR. A combination of complementary techniques is needed. The requirement that the glass foam scaffolds do not fulfil is toughness; glasses are brittle. Hybrids are a potential solution to this problem, as long as covalent coupling can be achieved between the organic and inorganic components and the chemistry nanostructure can be fully understood. This will push the boundaries of the advanced probe techniques even further.

References

1 Van Heest, A. & Swiontkowski, M. 1999 Bone-graft substitutes. *Lancet* **353**(Suppl. 1), SI28–SI29.

2 Lewandrowski, K. U., Gresser, J. D., Wise, D. L. & Trantol, D. J. 2000 Bioresorbable bone graft substitutes of different osteoconductivities: a histologic evaluation of osteointegration of poly(propylene glycol-co-fumaric acid)-based cement implants in rats. *Biomaterials* **21**, 757–764. (doi:10.1016/S0142-9612(99)00179-9)

3 Giannoudis, P. V., Dinopoulos, H. & Tsiridis, E. 2005 Bone substitutes: an update, injury-international. *J. Care Injured* **36**, S20–S27. (doi:10.1016/j.injury.2005.07.029)

4 Summers, B. N. & Eisenstein, S. M. 1989 Donor site pain from the ilium: a complication of the lumbar spine fusion. *J. Bone Joint Surg. B* **71**, 677–680.

5 Skaggs, D. L., Samuelson, M. A., Hale, J. M., Kay, R. M. & Tolo, V. T. 2000 Complications of posterior iliac crest bone grafting in spine surgery in children. *Spine* **25**, 2400–2402. (doi:10.1097/00007632-200009150-00021)

6 Salzman, N. P., Psallidopoulos, M., Prewett, A. B. & Oleary, R. 1993 Detection of HIV in bone allografts prepared from aids autopsy tissue. *Clin. Orthop. Relat. Res.* **292**, 384–390.

7 Carter, G. 1999 Harvesting and implanting allograft bone. *AORN J.* **70**, 660–670. quiz 672–666. (doi:10.1016/S0001-2092(06)62441-1)

8 Jones, J. R., Lin, S., Yue, S., Lee, P. D., Hanna, J. V., Smith, M. E. & Newport, R. J. 2010 Bioactive glass scaffolds for bone regeneration and their hierarchical characterisation. *Proc. Inst. Mech. Eng. H J. Eng. Med.* **224**, 1373–1387. (doi:10.1243/09544119JEIM836)

9 Hench, L. L., Splinter, R. J., Allen, W. C. & Greenlee, T. K. 1971 Bonding mechanisms at the interface of ceramic prosthetic materials. *J. Biomed. Mater. Res. Symp.* **5**, 25. (doi:10.1002/jbm.820050104)

10 Hench, L. L. 2006 The story of bioglass (R). *J. Mater. Sci. Mater. Med.* **17**, 967–978. (doi:10.1007/s10856-006-0432-z)

11 Cao, W. P. & Hench, L. L. 1996 Bioactive materials. *Ceramics Int.* **22**, 493–507. (doi:10.1016/0272-8842(95)00126-3)

12 Oonishi, H., Kushitani, S., Yasukawa, E., Iwaki, H., Hench, L. L., Wilson, J., Tsuji, E. I. & Sugihara, T. 1997 Particulate bioglass compared with hydroxyapatite as a bone graft substitute. *Clin. Orthop. Relat. Res.* **334**, 316–325.

13 Oonishi, H., Hench, L. L., Wilson, J., Sugihara, F., Tsuji, E., Matsuura, M., Kin, S., Yamamoto, T. & Mizokawa, S. 2003 Quantitative comparison of bone growth behavior in granules of Bioglass (R), A-W glass-ceramic, and hydroxyapatite. *J. Biomed. Mater. Res.* **51**, 37–46. (doi:10.1002/(SICI)1097-4636(200007)51:1<37::AID-JBM6>3.0.CO;2-T)

14 Chen, Q. Z., Thompson, I. D. & Boccaccini, A. R. 2006 45S5 Bioglass-derived glass-ceramic scaffolds for bone tissue engineering. *Biomaterials* **27**, 2414–2425. (doi:10.1016/j.biomaterials.2005.11.025)

15 Wu, Z. Y., Hill, R. G., Yue, S., Nightingale, D., Lee, P. D. & Jones, J. R. 2011 Melt-derived bioactive glass scaffolds produced by a gel-cast foaming technique. *Acta Biomater.* **7**, 1807–1816. (doi:10.1016/j.actbio.2010.11.041)

16 Fu, Q., Rahaman, M. N., Bal, B. S., Brown, R. F. & Day, D. E. 2008 Mechanical and *in vitro* performance of 13–93 bioactive glass scaffolds prepared by a polymer foam replication technique. *Acta Biomater.* **4**, 1854–1864. (doi:10.1016/j.actbio.2008.04.019)

17 Li, R., Clark, A. E. & Hench, L. L. 1919 An investigation of bioactive glass powders by sol–gel processing. *J. Appl. Biomater.* **2**, 231–239. (doi:10.1002/jab.770020403)

18 Sepulveda, P., Jones, J. R. & Hench, L. L. 2001 Characterization of melt-derived 45S5 and sol–gel-derived 58S bioactive glasses. *J. Biomed. Mater. Res.* **58**, 734–740. (doi:10.1002/jbm.10026)

19 Jones, J. R., Ehrenfried, L. M. & Hench, L. L. 2006 Optimising bioactive glass scaffolds for bone tissue engineering. *Biomaterials* **27**, 964–973. (doi:10.1016/j.biomaterials.2005.07.017)

20 Valliant, E. M. & Jones, J. R. 2011 Softening bioactive glass for bone regeneration: sol–gel hybrid materials. *Soft Matter* **7**, 5083–5095. (doi:10.1039/c0sm01348j)

21 Jones, J. R. & Hench, L. L. 2003 Regeneration of trabecular bone using porous ceramics. *Curr. Opin. Solid State Mater. Sci.* **7**, 301–307. (doi:10.1016/j.cossms.2003.09.012)

22 Jones, J. R., Lee, P. D. & Hench, L. L. 2006 Hierarchical porous materials for tissue engineering. *Phil. Trans. R. Soc. A* **364**, 263–281. (doi:10.1098/rsta.2005.1689)

23 Hulbert, S. F., Morrison, S. J. & Klawitte, J. J. 1972 Tissue reaction to 3 ceramics of porous and non-porous structures. *J. Biomed. Mater. Res.* **6**, 347–374. (doi:10.1002/jbm.820060505)

24 Mackenzie, J. D. 1988 Applications of the sol–gel process. *J. Non-Cryst. Solids* **100**, 162–168. (doi:10.1016/0022-3093(88)90013-0)

25 Saravanapavan, P. & Hench, L. L. 2003 Mesoporous calcium silicate glasses. I. Synthesis. *J. Non-Cryst. Solids* **318**, 1–13. (doi:10.1016/S0022-3093(02)01864-1)

26 Saravanapavan, P. & Hench, L. L. 2001 Low-temperature synthesis, structure, and bioactivity of gel-derived glasses in the binary CaO–SiO_2 system. *J. Biomed. Mater. Res.* **54**, 608–618. (doi:10.1002/1097-4636(20010315)54:4<608::AID-JBM18>3.0.CO;2-U)

27 Jones, J. R., Kemp, T. F. & Smith, M. E. 2006 Effect of OH content on the bioactivity of sol–gel derived glass foam scaffolds. *Bioceramics* **18**(Pts 1 and 2), 309–311; 1031–1034. (doi:10.4028/www.scientific.net/KEM.309-311.1031)

28 Labbaf, S., Tsigkou, O., Muller, K. H., Stevens, M. M., Porter, A. E. & Jones, J. R. 2011 Spherical bioactive glass particles and their interaction with human mesenchymal stem cells *in vitro. Biomaterials* **32**, 1010–1018. (doi:10.1016/j.biomaterials.2010.08.082)

29 Hench, L. L. & West, J. K. 1990 The sol–gel process. *Chem. Rev.* **90**, 33–72. (doi:10.1021/cr00099a003)

30 Duran, A., Serna, C., Fornes, V. & Fernandez Navarro, J. M. 1986 Structural considerations about SiO_2 glasses prepared by sol–gel. *J. Non-Cryst. Solids* **82**, 69–77. (doi:10.1016/0022-3093(86)90112-2)

31 Colby, M. W., Osaka, A. & Mackenzie, J. D. 1986 Effects of temperature on formation of silica gel. *J. Non-Cryst. Solids* **82**, 37–41. (doi:10.1016/0022-3093(86)90108-0)

32 Sepulveda, P., Jones, J. R. & Hench, L. L. 2002 Bioactive sol–gel foams for tissue repair. *J. Biomed. Mater. Res.* **59**, 340–348. (doi:10.1002/jbm.1250)

33 Scherer, G. W. & Brinker, C. J. 1990 *Sol–gel science: the physics and chemistry of sol–gel processing.* New York, NY: Academic Press.

34 Xynos, I. D., Edgar, A. J., Buttery, L. D. K., Hench, L. L. & Polak, J. M. 2001 Gene-expression profiling of human osteoblasts following treatment with the ionic products of Bioglass (R) 45S5 dissolution. *J. Biomed. Mater. Res.* **55**, 151–157. (doi:10.1002/1097-4636(200105)55:2<151::AID-JBM1001>3.0.CO;2-D)

35 Xynos, I. D., Hukkanen, M. V. J., Batten, J. J., Buttery, L. D., Hench, L. L. & Polak, J. M. 2000 Bioglass (R) 45S5 stimulates osteoblast turnover and enhances bone formation *in vitro*: implications and applications for bone tissue engineering. *Calcified Tissue Int.* **67**, 321–329. (doi:10.1007/s002230001134)

36 Hench, L. L. & Thompson, I. 2010 Twenty-first century challenges for biomaterials. *J. R. Soc. Interface* **7**, S379–S391. (doi:10.1098/rsif.2010.0151.focus)

37 Hench, L. L., Day, D. E., Höland, W. & Rheinberger, V. M. 2010 Glass and medicine. *Int. J. Appl. Glass Sci.* **1**, 104–117. (doi:10.1111/j.2041-1294.2010.00001.x)

38 Saravanapavan, P., Jones, J. R., Pryce, R. S. & Hench, L. L. 2003 Bioactivity of gel-glass powders in the $CaO–SiO_2$ system: a comparison with ternary ($CaO-P_2O_5–SiO_2$) and quaternary glasses ($SiO_2–CaO–P_2O_5–Na_2O$). *J. Biomed. Mater. Res. A* **66**, 110–119. (doi:10.1002/jbm.a.10532)

39 Hench, L. L. 1991 Bioceramics: from concept to clinic. *J. Am. Ceramic Soc.* **74**, 1487–1510. (doi:10.1111/j.1151-2916.1991.tb07132.x)

40 Hill, R. 1996 An alternative view of the degradation of bioglass. *J. Mater. Sci. Lett.* **15**, 1122–1125. (doi:10.1007/BF00539955)

41 Vallet-Regi, M., Ragel, C. V. & Salinas, A. J. 2003 Glasses with medical applications. *Eur. J. Inorg. Chem.* **2003**, 1029–1042. (doi:10.1002/ejic.200390134)

42 Elgayar, I., Aliev, A. E., Boccaccini, A. R. & Hill, R. G. 2005 Structural analysis of bioactive glasses. *J. Non-Cryst. Solids* **351**, 173–183. (doi:10.1016/j.jnoncrysol.2004.07.067)

43 Lin, S., Ionescu, C., Pike, K. J., Smith, M. E. & Jones, J. R. 2009 Nanostructure evolution and calcium distribution in sol–gel derived bioactive glass. *J. Mater. Chem.* **19**, 1276–1282. (doi:10.1039/b814292k)

44 Kim, H.-M., Miyaji, F., Kokubo, T. & Nakamura, T. 1996 Preparation of bioactive Ti and its alloys via simple chemical surface treatment. *J. Biomed. Mater. Res.* **32**, 409–417. (doi:10.1002/(SICI)1097-4636(199611)32:3<409::AID-JBM14>3.0.CO;2-B)

45 Kawai, T., Ohtsuki, C., Kamitakahara, M., Hosoya, K., Tanihara, M., Miyazaki, T., Sakaguchi, Y. & Konagaya, S. 2007 *In vitro* apatite formation on polyamide containing carboxyl groups modified with silanol groups. *J. Mater. Sci. Mater. Med.* **18**, 1037–1042. (doi:10.1007/s10856-006-0081-2)

46 Newport, R. J., Skipper, L. J., Carta, D., Pickup, D. M., Sowrey, F. E., Smith, M. E., Saravanapavan, P. & Hench, L. L. 2006 The use of advanced diffraction methods in the study of the structure of a bioactive calcia: silica sol–gel glass. *J. Mater. Sci. Mater. Med.* **17**, 1003–1010. (doi:10.1007/s10856-006-0436-8)

47 Skipper, L. J., Sowrey, F. E., Rashid, R., Newport, R. J., Lin, Z. & Smith, M. E. 2005 X-ray diffraction and solid state NMR studies of the growth of hydroxyapatite on bioactive calcia: silica sol–gel glasses. *Phys. Chem. Glasses* **46**, 372–376.

48 Lin, S., Ionescu, C., Baker, S., Smith, M. E. & Jones, J. R. 2010 Characterisation of the inhomogeneity of sol–gel-derived SiO$_2$–CaO bioactive glass and a strategy for its improvement. *J. Sol-Gel Sci. Technol.* **53**, 255–262. (doi:10.1007/s10971-009-2085-0)

49 Yue, S., Lee, P. D., Poologasundarampillai, G., Yao, Z. Z., Rockett, P., Devlin, A. H., Mitchell, C. A., Konerding, M. A. & Jones, J. R. 2010 Synchrotron X-ray microtomography for assessment of bone tissue scaffolds. *J. Mater. Sci. Mater. Med.* **21**, 847–853. (doi:10.1007/s10856-009-3888-9)

50 Rehman, I., Hench, L. L., Bonfield, W. & Smith, R. 1994 Analysis of surface-layers on bioactive glasses. *Biomaterials* **15**, 865–870. (doi:10.1016/0142-9612(94)90044-2)

51 Martin, R. A., Twyman, H., Qiu, D., Knowles, J. C. & Newport, R. J. 2009 A study of the formation of amorphous calcium phosphate and hydroxyapatite on melt quenched Bioglass(A (R)) using surface sensitive shallow angle X-ray diffraction. *J. Mater. Sci. Mater. Med.* **20**, 883–888. (doi:10.1007/s10856-008-3661-5)

52 Mead, R. N. & Mountjoy, G. 2006 Modeling the local atomic structure of bioactive sol–gel-derived calcium silicates. *Chem. Mater.* **18**, 3956–3964. (doi:10.1021/cm0527975)

53 FitzGerald, V., Drake, K. O., Jones, J. R., Smith, M. E., Honkimaki, V., Buslaps, T., Kretzschmer, M. & Newport, R. J. 2007 *In situ* high-energy X-ray diffraction study of a bioactive calcium silicate foam immersed in simulated body fluid. *J. Synchrotron Radiat.* **14**, 492–499. (doi:10.1107/S0909049507042173)

54 Skipper, L. J., Sowrey, F. E., Pickup, D. M., Drake, K. O., Smith, M. E., Saravanapavan, P., Hench, L. L. & Newport, R. J. 2005 The structure of a bioactive calcia-silica sol–gel glass. *J. Mater. Chem.* **15**, 2369–2374. (doi:10.1039/b501496d)

55 Newport, R. J., Skipper, L. J., FitzGerald, V., Pickup, D. M., Smith, M. E. & Jones, J. R. 2007 *In vitro* changes in the structure of a bioactive calcia-silica sol–gel glass explored using isotopic substitution in neutron diffraction. *J. Non-Cryst. Solids* **353**, 1854–1859. (doi:10.1016/j.jnoncrysol.2007.02.015)

56 Skipper, L. J. *et al.* 2004 Structural studies of bioactivity in sol–gel-derived glasses by X-ray spectroscopy. *J. Biomed. Mater. Res. A* **70**, 354–360. (doi:10.1002/jbm.a.30093)

57 Skipper, L. J., Sowrey, F. E., Pickup, D. M., Newport, R. J., Drake, K. O., Lin, Z. H., Smith, M. E., Saravanapavan, P. & Hench, L. L. 2005 The atomic-scale interaction of bioactive glasses with simulated body fluid. *Cross-Discipl. Appl. Res. Mater. Sci. Technol.* **480–481**, 21–26. (doi:10.4028/www.scientific.net/MSF.480-481.21)

58 Mead, R. N. & Mountjoy, G. 2006 Molecular dynamics modelling of the structure of bioactive (CaO)(0.3)(SiO$_2$)(0.7) sol–gel. *Adv. Mater. Forum Iii* **514–516**(Pts 1 and 2), 1059–1063. (doi:10.4028/www.scientific.net/MSF.514-516.1059)

59 Lin, Z. J., Smith, M. E., Sowrey, F. E. & Newport, R. J. 2004 Probing the local structural environment of calcium by natural-abundance solid-state Ca-43 NMR. *Phys. Rev. B* **69**, 224107. (doi:10.1103/PhysRevB.69.224107)

60 Sears, V. F. 1992 Neutron scattering lengths and cross sections. *Neutron News* **3**, 26–37. (doi:10.1080/10448639208218770)

61 FitzGerald, V., Martin, R. A., Jones, J. R., Qiu, D., Wetherall, K. M., Moss, R. M. & Newport, R. J. 2009 Bioactive glass sol–gel foam scaffolds: evolution of nanoporosity during processing and in situ monitoring of apatite layer formation using small- and wide-angle X-ray scattering. *J. Biomed. Mater. Res. A* **91**, 76–83. (doi:10.1002/jbm.a.32206)

62 Salinas, A. J., Martin, A. I. & Vallet-Regi, M. 2002 Bioactivity of three CaO-P$_2$O$_5$–SiO$_2$ sol–gel glasses. *J. Biomed. Mater. Res.* **61**, 524–532. (doi:10.1002/jbm.10229)

63 Vallet-Regi, M., Arcos, D. & Perez-Pariente, J. 2003 Evolution of porosity during *in vitro* hydroxycarbonate apatite growth in sol–gel glasses. *J. Biomed. Mater. Res.* **51**, 23–28. (doi:10.1002/(SICI)1097-4636(200007)51:1<23::AID-JBM4>3.0.CO;2-B)

64 Vallet-Regi, M., Romero, A. M., Ragel, C. V. & LeGeros, R. Z. 1999 XRD, SEM-EDS, and FTIR studies of *in vitro* growth of an apatite-like layer on sol–gel glasses. *J. Biomed. Mater. Res.* **44**, 416–421. (doi:10.1002/(SICI)1097-4636(19990315)44:4<416::AID-JBM7>3.0.CO;2-S)

65 Roman, J., Padilla, S. & Vallet-Regi, M. 2003 Sol–gel glasses as precursors of bioactive glass ceramics. *Chem. Mater.* **15**, 798–806. (doi:10.1021/cm021325c)

66 Lao, J., Nedelec, J. M., Moretto, P. & Jallot, E. 2006 Micro-PIXE characterization of interactions between a sol–gel derived bioactive glass and biological fluids. *Nucl. Instr. Methods Phys. Res. B, Beam Interact. Mater. At.* **245**, 511–518. (doi:10.1016/j.nimb.2005.12.049)

67 Lao, J., Nedelec, J. M., Moretto, P. & Jallot, E. 2008 Micro-PIXE-RBS methods highlighting the influence of phosphorus on the *in vitro* bioactivity of sol–gel derived glass particles in the SiO_2–CaO–P_2O_5 system. *Nucl. Instr. Methods Phys. Res. B, Beam Interact. Mater. At.* **266**, 2412–2417. (doi:10.1016/j.nimb.2008.03.013)

68 Courtheoux, L., Lao, J., Nedelec, J. M. & Jallot, E. 2008 Controlled bioactivity in zinc-doped sol–gel-derived binary bioactive glasses. *J. Phys. Chem. C* **112**, 13 663–13 667. (doi:10.1021/jp8044498)

69 Lao, J., Nedelec, J. M. & Jallot, E. 2008 New insights in the physico-chemistry at the interface between sol–gel derived bioactive glasses and biological medium: A PIXE-RBS study (vol 112C, pg 9418, 2008). *J. Phys. Chem. C* **112**, 14 220–14 220. (doi:10.1021/jp8061898)

70 Martin, R. A. *et al.* 2011 An X-ray micro-fluorescence study to investigate the distribution of Al, Si, P and Ca ions in the surrounding soft tissue after implantation of a calcium phosphate-mullite ceramic composite in a rabbit animal model. *J. Mater. Sci. Mater. Med.* **22**, 2537–2543. (doi:10.1007/s10856-011-4428-y)

71 Atwood, R. C., Jones, J. R., Lee, P. D. & Hench, L. L. 2004 Analysis of pore interconnectivity in bioactive glass foams using X-ray microtomography. *Scr. Mater.* **51**, 1029–1033. (doi:10.1016/j.scriptamat.2004.08.014)

72 Jones, J. R., Poologasundarampillai, G., Atwood, R. C., Bernard, D. & Lee, P. D. 2007 Non-destructive quantitative 3D analysis for the optimisation of tissue scaffolds. *Biomaterials* **28**, 1404–1413. (doi:10.1016/j.biomaterials.2006.11.014)

73 Yue, S., Lee, P. D., Poologasundarampillai, G. & Jones, J. R. 2011 Evaluation of 3-D bioactive glass scaffolds dissolution in a perfusion flow system with X-ray microtomography. *Acta Biomater.* **7**, 2637–2643. (doi:10.1016/j.actbio.2011.02.009)

74 Dong, H. & Blunt, M. J. 2009 Pore-network extraction from micro-computerized-tomography images. *Phys. Rev. E, Stat. Nonlinear Soft Matter Phys.* **80**, 036307. (doi:10.1103/PhysRevE.80.036307)

75 Dave, B. C., Soyez, H., Miller, J. M., Dunn, B., Valentine, J. S. & Zink, J. I. 1995 Synthesis of protein-doped sol–gel SiO_2 thin films: evidence for rotational mobility of encapsulated cytochrome c. *Chem. Mater.* **7**, 1431–1434. (doi:10.1021/cm00056a003)

76 Xie, Z.-P., Zhang, C.-Q., Yi, C.-Q., Qiu, J.-J., Wang, J.-Q. & Zhou, J. *In vivo* study effect of particulate bioglass (R) in the prevention of infection in open fracture fixation. *J. Biomed. Mater. Res. B Appl. Biomater.* **90B**, 195–201. (doi:10.1002/jbm.b.31273)

77 Bellantone, M., Williams, H. D. & Hench, L. L. 2002 Broad-spectrum bactericidal activity of Ag_2O-doped bioactive glass. *Antimicrob. Agents Chemother.* **46**, 1940–1945. (doi:10.1128/AAC.46.6.1940-1945.2002)

78 Jones, J. R., Ehrenfried, L. M., Saravanapavan, P. & Hench, L. L. 2006 Controlling ion release from bioactive glass foam scaffolds with antibacterial properties. *J. Mater. Sci. Mater. Med.* **17**, 989–996. (doi:10.1007/s10856-006-0434-x)

79 Lenza, R. F. S., Jones, J. R., Vasconcelos, W. L. & Hench, L. L. 2003 *In vitro* release kinetics of proteins from bioactive foams. *J. Biomed. Mater. Res. A* **67**, 121–129. (doi:10.1002/jbm.a.10042)

80 Karakoti, A. S., Tsigkou, O., Yue, S., Lee, P. D., Stevens, M. M., Jones, J. R. & Seal, S. 2010 Rare earth oxides as nanoadditives in 3-D nanocomposite scaffolds for bone regeneration. *J. Mater. Chem.* **20**, 8912–8919. (doi:10.1039/c0jm01072c)

81 Poologasundarampillai, G., Ionescu, C., Tsigkou, O., Murugesan, M., Hill, R. G., Stevens, M. M., Hanna, J. V., Smith, M. E. & Jones, J. R. 2010 Synthesis of bioactive class II poly(gamma-glutamic acid)/silica hybrids for bone regeneration. *J. Mater. Chem.* **20**, 8952–8961. (doi:10.1039/c0jm00930j)

82 Mahony, O., Tsigkou, O., Ionescu, C., Minelli, C., Ling, L., Hanly, R., Smith, M. E., Stevens, M. M. & Jones, J. R. 2010 Silica-gelatin hybrids with tailorable degradation and

mechanical properties for tissue regeneration. *Adv. Funct. Mater.* **20**, 3835–3845. (doi:10.1002/adfm.201000838)

83 Babonneau, F., Baccile, N., Laurent, G., Maquet, J., Azaïs, T., Gervais, C. & Bonhomme, C. 2009 Solid-state nuclear magnetic resonance: a valuable tool to explore organic–inorganic interfaces in silica-based hybrid materials. *C. R. Chim.* **13**, 58–68. (doi:10.1016/j.crci.2009.08.001)

84 Alonso, B. *et al.* 2010 Perspectives in 1H, 14N and 81Br solid-state NMR studies of interfaces in materials textured by self-assembled amphiphiles. *C. R. Chim.* **13**, 431–442. (doi:10.1016/j.crci.2009.10.002)

85 Pedone, A., Charpentier, T., Malavasi, G. & Menziani, M. C. 2010 New insights into the atomic structure of 45S5 bioglass by means of solid-state NMR spectroscopy and accurate first-principles simulations. *Chem. Mater.* **22**, 5644–5652. (doi:10.1021/cm102089c)

86 Yu, B., Poologasundarampillai, G., Turdean-Ionescu, C., Smith, M. E. & Jones, J. R. 2011 A new calcium source for bioactive sol–gel hybrids. *Bioceramics Dev. Appl.* **1**, 1–3. (doi:10.4303/bda/D110178)